Journal of Hydrology 585 (2020) 124777

Contents lists available at ScienceDirect

Journal of Hydrology

journal homepage: www.elsevier.com/locate/jhydrol

Research papers

Modeling the processes of soil moisture in regulating microbial and carbon-nitrogen cycling

Gangsheng Wang[a,*], Wenjuan Huang[b,c], Guoyi Zhou[d], Melanie A. Mayes[e], Jizhong Zhou[a,f,g]

[a] Institute for Environmental Genomics and Department of Microbiology & Plant Biology, University of Oklahoma, Norman, OK 73019, USA
[b] Key Laboratory of Vegetation Restoration and Management of Degraded Ecosystems, South China Botanical Garden, Chinese Academy of Sciences, Guangzhou 510650, China
[c] Department of Ecology, Evolution, and Organismal Biology, Iowa State University, Ames, IA 50011, USA
[d] School of Applied Meteorology, Nanjing University of Information Science & Technology, Nanjing 210044, China
[e] Environmental Sciences Division & Climate Change Science Institute, Oak Ridge National Laboratory, Oak Ridge, TN 37831-6301, USA
[f] Earth and Environmental Sciences, Lawrence Berkeley National Laboratory, Berkeley, CA 94270, USA
[g] State Key Joint Laboratory of Environment Simulation and Pollution Control, School of Environment, Tsinghua University, Beijing 100084, China

ARTICLE INFO

Keywords:
Dynamic data
Microbial modeling
Microbial dormancy
Soil carbon and nitrogen
Soil microbe
Soil moisture

ABSTRACT

Soil carbon (C) and nitrogen (N) cycles and their complex responses to hydro-climatic forcing have gained increasing attention. While the temperature effects have been intensively studied, soil moisture response functions (SMRFs) are not well documented for various microbial and enzymatic processes due to the difficulties in directly measuring and differentiating the moisture effects on various processes. Here we extended our C-only Microbial-ENzyme Decomposition (MEND) model to the C-N coupled MEND model with flexible element stoichiometry. Our model calibration showed good agreement between simulated and observed C:N ratios in soil organic matter and microbial biomass, as well as the ammonium and nitrate concentrations. We show that the selection of SMRFs for specific biogeochemical processes could result in significant differences in model simulated microbial and C-N processes. In particular, it is essential to account for the soil moisture effects on microbial dormancy and resuscitation, as the changes in microbial physiology under favorable or stressful conditions will exert strong controls on soil C and N dynamics. We also advocate the utilization of dynamic (time-variant) data (e.g., litter input, N deposition, soil temperature and moisture), instead of time-invariant data, to drive model simulations and analyses. Dynamic forcing data (particularly dynamic soil moisture) better represent the real-world climate and environmental conditions, which could facilitate more realistic modeling and understanding of soil C and nutrient cycling in a changing world.

1. Introduction

Soil carbon (C) and nutrient cycles and their complex responses to hydro-climatic forcing have gained increasing attention during the last two decades (Bradford et al., 2016; Campo and Merino, 2016; Crowther et al., 2016; Manzoni et al., 2004). While the temperature effects have been intensively studied (Allison et al., 2010; Carey et al., 2016; Crowther et al., 2016; Frey et al., 2013; Tang and Riley, 2015), it remains a challenge to separate the effects from both soil temperature and moisture (Campo and Merino, 2016; Davidson et al., 2012; Ohashi et al., 2008; Rowland et al., 2014). The effect of soil moisture on soil C and nutrient dynamics cannot be neglected because soil microbes mediate these processes and fluctuations in microbial activities in response to soil moisture changes are ubiquitous (Manzoni et al., 2012a). When soil becomes drier, the microbial metabolic activity generally is depressed, which might reduce heterotrophic respiration and nitrogen (N) mineralization (Schimel et al., 2007). A reduction of 10% in soil water content (SWC) led to a 10–80% decrease in β-glucosidase activity in Mediterranean evergreen forests (Sardans and Penuelas, 2005). The β-glucosidase and endo-glucanase activities showed significantly higher correlations with soil moisture than temperature and pH in the study by Criquet et al. (2002). However, saturated water conditions could reduce the phenol oxidases activity due to oxygen deficiency (Freeman et al., 2001). Therefore, quantifying the soil moisture effects in ecosystem modeling helps to understand the underlying mechanisms regulating soil C and nutrient cycling.

The incorporation of soil moisture response functions (SMRFs) significantly improved the modeling of soil organic matter (SOM)

* Corresponding author.
E-mail address: wanggs@ou.edu (G. Wang).

https://doi.org/10.1016/j.jhydrol.2020.124777

Available online 02 March 2020

decomposition and soil respiration (Ise and Moorcroft, 2006; Liang et al., 2019), as the activities of lignocellulose-degrading enzymes and respiration were highly affected by the changes in moisture content (Baldrian and Stursova, 2011). Current soil C and ecosystem models usually use SMRFs to modify SOM decomposition rates (Ma and Shaffer, 2001; Shi et al., 2015; Wu and McGechan, 1998) or microbial respiration rates (Moyano et al., 2013). Soil moisture availability will influence microbial growth, maintenance, mortality, reactivation and dormancy, and enzyme activities (Baldrian and Stursova, 2011; Wang et al., 2019), all of which underlie the mechanisms controlling microbially-mediated soil biogeochemical processes. For example, microbes (mainly bacteria) tend to become dormant under low moisture conditions (Wang et al., 2019; Wang et al., 2015). The same SWC in different organic solvents or soils could result in completely different amounts of water bound on the enzymes (Zaks and Klibanov, 1988). Thus water activity or potential, instead of SWC, has been widely used in SMRFs to characterize the effect of water on microbial and enzyme activities (Goujard et al., 2009; Halling, 1994; Manzoni et al., 2012b; Wang et al., 2019). Unfortunately, SMRFs are not well documented for various microbial and enzymatic processes due to the difficulties in directly measuring the effects on different processes (Wallenstein and Weintraub, 2008). Our previous model-data fusion study in subtropical forests showed higher microbial biomass and active fraction of microbes in the wet season than in the dry season, in which distinct SMRFs were adopted and parameterized for different processes including oxidative and hydrolytic decomposition, microbial mortality, dormancy and resuscitation (Wang et al., 2019). Different SMRFs may impose different effects on microbial and enzyme activities, which further alter the mineralization of soil organic C and N, the immobilization of inorganic N, as well as the nitrification and denitrification processes. However, it remains unclear whether an alternative SMRF would significantly affect the C-N processes in soils.

In addition, current testing and evaluation of microbially-enabled biogeochemical models often use steady-state analyses with time-invariant forcing data (e.g., constant soil temperature, moisture and litter input) as such model simulations are easy to implement and convenient for analyses (e.g., Allison et al., 2010; Sulman et al., 2018; Wang et al., 2013). The findings from these simplified analyses have been assumed to be capable of characterizing ecosystem responses to environmental perturbations or changes, such as positive, negative, or neutral responses to warming, drought, or litter addition (Hagerty et al., 2014; Sulman et al., 2018). However, if the model behaviors are qualitatively different (e.g., positive vs. negative effect) between simulations with constant and dynamic data, we need to be cautious in extrapolating the findings based on constant data, as these climatic and environmental forcings usually vary with time. For this reason, there is a need to understand if model behaviors will be consistent when a model is driven by constant or dynamic forcing data.

In order to answer these questions, we extended our C-only Microbial-ENzyme Decomposition (MEND) model to the C-N coupled MEND model with flexible elemental stoichiometry (Buchkowski et al., 2015; Sistla and Schimel, 2012). We focused on the selection of SMRFs for different biogeochemical processes and their impacts on soil C and N cycling. We also examined if the MEND modeling with dynamic forcings, particularly time-variant soil moisture, could generate substantially different results from those driven by time-invariant data.

2. Materials and methods

2.1. Carbon-Nitrogen coupled MEND model

We developed a new version of the MEND model, i.e., the C-N coupled MEND model (Fig. 1). The C-only MEND describes the SOM decomposition processes by explicitly representing relevant microbial and enzymatic physiology (Wang et al., 2019; Wang et al., 2015; Wang et al., 2013). The SOM pool consists of two particulate organic matter (POM) pools and one mineral-associated organic matter (MOM) pool. The two POMs are decomposed by oxidative and hydrolytic enzymes, respectively. The MOM is decomposed by a general enzyme group EM. The C-N coupled MEND represents additional C-N transformation processes: soil organic N (SON) decomposition coupled to the soil organic C (SOC) decomposition, microbial N mineralization and immobilization, nitrification, denitrification (Wang and Chen, 2013), and nitrifier denitrification (Wrage-Mönnig et al., 2018; Zhu et al., 2013). Model state variables, governing equations, component fluxes and parameters are described in Tables 1–4, respectively.

In contrast to traditional models that use fixed SOM C:N ratios (Bonan et al., 2013; Thornton and Rosenbloom, 2005), we use flexible stoichiometry (i.e., time-variant C:N ratio) for SOM and microbial biomass pools to more realistically represent the adaption of microbes in response to the stoichiometric imbalance of available resources (Fanin et al., 2017). As for the enzyme pools, a fixed C:N ratio (=3) is used based on Schimel and Weinstraub (2003). Generally, the SON flux will follow the SOC flux according to the C:N ratio in the upstream (source) pool (see Eq. 13 in Table 2). The C:N ratios in the SOM pools (including POM_O, POM_H, MOM, QOM, DOM) will be regulated by the litter input, C-N fluxes from upstream pools, and/or microbial turnover. The C:N ratio in the microbial biomass pool is self-regulated by the DOM uptake, heterotrophic respiration (R_h), N mineralization and immobilization. R_h is mainly controlled by the intrinsic C use efficiency (Y_g or intrinsic CUE) (see Eqs. 27–31). In addition to the availability of DON and mineral N (NH_4^+ and NO_3^-), we define an intrinsic N use efficiency (YN_g or intrinsic NUE, see Eq. 38 in Table 3) to modify N mineralization rate (Eq. 37) and immobilization rate (Eqs. 35–36). In Eq. 38, we first assume a conservative C:N range (i.e., between $CN_{BA,\min}$ and $CN_{BA,\max}$) to represent the stoichiometric plasticity of microbial communities (Cleveland and Liptzin, 2007; Fanin et al., 2017; Zechmeister-Boltenstern et al., 2015). Intrinsic NUE (YN_g in Eq. 38) will increase with increasing microbial C:N ratio (CN_{BA}), with YN_g being 0 when $CN_{BA} \le CN_{BA,\min}$ (C-limited) and YN_g approaching 1 when $CN_{BA} \ge CN_{BA,\max}$ (N-limited). This means that N mineralization rate will decrease, and N immobilization rate will increase when microorganisms become more N limited, resulting in higher YN_g (Mooshammer et al., 2014).

A model parameter (reaction rate) in MEND may be modified by soil moisture, temperature, and/or pH (Wang et al., 2019). MEND represents nitrification, denitrification, microbial dormancy, resuscitation, and mortality and enzymatic decomposition in response to changes in moisture, as well as shifts in microbial and enzymatic activities with changing temperature (Wang et al., 2019). The intrinsic CUE (Y_g in Table 4) decreases with increasing temperature following a linear function (Li et al., 2019; Wang et al., 2019). The temperature sensitivities of microbial and enzyme activities are modeled by the Q_{10} method (Wang et al., 2012) or the Arrhenius equation characterized by the activation energy (Wang et al., 2013). The following section describes the SMRFs for different processes as soil moisture effect is the focus of this study.

2.2. Soil moisture response functions

We use different SMRFs (Wang et al., 2019) to describe the influences of soil moisture on the enzyme-mediated SOM decomposition processes, microbial mortality, microbial dormancy and resuscitation, nitrification and denitrification.

(1) The SMRF for SOM decomposition by oxidative enzymes is adapted from Hansen et al. (1990). (Fig. 2a)

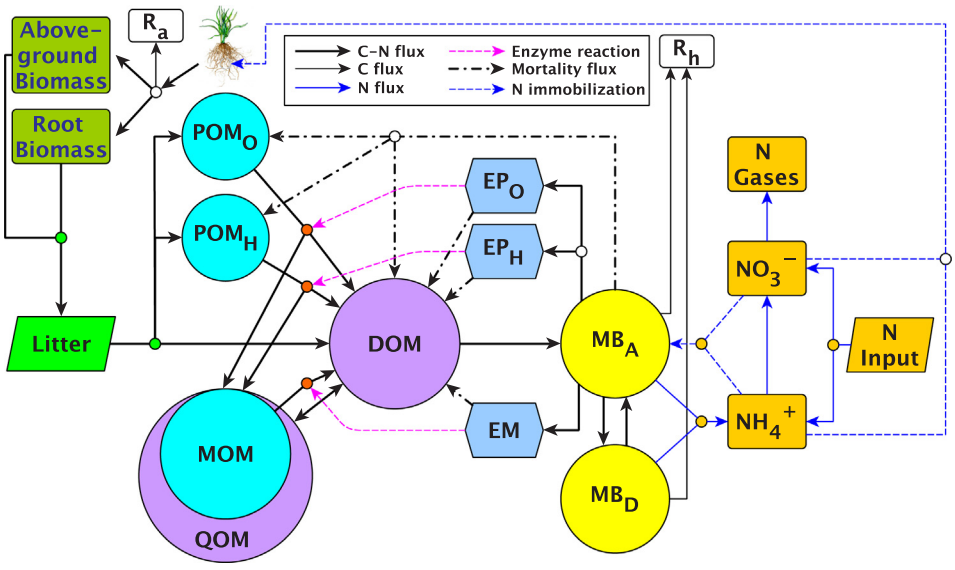

Fig. 1. The C-N coupled Microbial-ENzyme Decomposition (MEND) model. R_a and R_h are autotrophic and heterotrophic respiration, respectively. POM_O and POM_H are particulate organic matter (POM) decomposed by oxidative (EP_O) and hydrolytic enzymes (EP_H), respectively. MOM is mineral-associated OM, which is decomposed by a mixed enzyme group EM. Dissolved OM (DOM) interacts with the active layer of MOM (QOM) through sorption and desorption. Litter enters POM_O, POM_H, and DOM. Microbes consist of active (MB_A) and dormant microbes (MB_D). DOM can be assimilated by MB_A. Mineral N input enters NH_4^+ and NO_3^- that can be immobilized by microbes and taken up by plant roots.

Table 1
Soil carbon (C) and nitrogen (N) pools (state variables) in the MEND model.

ID	Soil C and/or N pool	Pool Name	Variable name in equations
1	Particulate organic matter (POM) decomposed by oxidative enzymes	POM_O	C pool: P_O; N pool: PN_O
2	POM decomposed by hydrolytic enzymes	POM_H	P_H; PN_H
3	Mineral-associated organic matter	MOM	*M*; *MN*
4	Dissolved organic matter	DOM	*D*; *DN*
5	Active MOM interacting with DOM	QOM	*Q*; *QN*
6	Active microbial biomass	MB_A	*BA*; *BAN*
7	Dormant microbial biomass	MB_D	*BD*; *BDN*
8	Oxidative enzymes decomposing POM_O	EP_O	EP_O; EPN_O
9	Hydrolytic enzymes decomposing POM_H	EP_H	EP_H; EPN_H
10	Enzymes decomposing MOM	EM	*EM*; *EMN*
11	Ammonium	NH_4^+	NH_4
12	Nitrate	NO_3^-	NO_3

$$f_{lig}(\psi) = \begin{cases} 0, \psi \le -10^{2.5} \\ 0.625 - 0.25 \times \log_{10}(-\psi), -10^{2.5} < \psi \le -10^{1.5} \\ 1, -10^{1.5} < \psi \le -10^{-2.5} \\ [2.5 + 0.4 \times \log_{10}(-\psi)]/1.5, -10^{-2.5} < \psi \le -10^{-4} \\ 0.6, \psi > -10^{-4} \end{cases} \quad (42)$$

where ψ is the soil water potential (SWP) in units of MPa and $f_{lig}(\psi)$ denotes the SMRF for the POM decomposition by oxidative enzymes.

(2) The SMRF for SOM decomposition by hydrolytic enzymes is based on Manzoni et al. (2012a) (Fig. 2a)

$$f_{cel}(\psi) = \begin{cases} 0, \psi \le \psi_{min} \\ 1 - \left[\frac{\ln(\psi / \psi_{FC})}{\ln(\psi_{min} / \psi_{FC})}\right]^b, \psi_{min} < \psi \le \psi_{FC} \\ 1, \psi > \psi_{FC} \end{cases} \quad (43)$$

where $f_{cel}(\psi)$ denotes the SMRF for the POM decomposition by hydrolytic enzymes or the decomposition of MOM, ψ_{FC} ($= -0.033$ MPa) is the SWP at field capacity, ψ_{min} is the microbial stress threshold SWP, and b is a shape parameter. The values of ψ_{min} and b for soil or litter in different biomes are adapted from Manzoni et al. (2012a).

(3) The SMRFs for microbial mortality, dormancy & resuscitation (Manzoni et al., 2014; Wang et al., 2019) are also shown in Fig. 2a.

Soil water potential greatly affects the microbial dormancy and reactivation processes and various sigmoidal-type switching functions have been proposed to quantify these effects (Manzoni et al., 2014; Wang et al., 2019), e.g., the response functions used to modify the dormancy ($f_{A2D}(\psi)$) and the reactivation ($f_{D2A}(\psi)$) can be expressed as

$$f_{A2D}(\psi) = \frac{(-\psi)^\omega}{(-\psi)^\omega + (-\psi_{A2D})^\omega} \quad (44)$$

$$f_{D2A}(\psi) = \frac{(-\psi_{D2A})^\omega}{(-\psi)^\omega + (-\psi_{D2A})^\omega} \quad (45)$$

where ψ is the SWP (MPa) and the exponent ω describes the steepness of the curve. ψ_{A2D} and ψ_{D2A} are critical SWPs depending on the osmolyte synthesis strategy (Manzoni et al., 2014). We also use $f_{A2D}(\psi)$ to modify microbial mortality rate.

(4) The SMRFs for nitrification and denitrification (Muller, 1999) are shown in Fig. 2b.

$$f(WFP) = \begin{cases} 0 & WFP \leqslant WFP_1 \\ a_+ + b_+ \cdot WFP & WFP_1 < WFP \leqslant WFP_2 \\ 1 & WFP_2 < WFP \leqslant WFP_3 \\ a_- + b_- \cdot WFP & WFP_3 < WFP \leqslant WFP_4 \\ 0 & WFP > WFP_4 \end{cases} \quad (46)$$

where $WFP = \theta/\phi$ is water-filled pore space (θ and ϕ denotes the volumetric water content and soil porosity, respectively); a_+ and b_+ are intercept and slope of linear regression for increasing activity (i.e., $b_+ > 0$); and a_- and b_- are intercept and slope of linear regression for decreasing activity (i.e., $b_- < 0$) (Wang and Chen, 2013). The values for WFP_i, ($i = 1, 2, 3, 4$) and a_+, b_+, a_-, b_- are from Muller (1999).

2.3. Study site and data collection

We compiled data from a three-year duration field experiment in a subtropical monsoon evergreen broadleaf forest (BF) within the Dinghushan Biosphere Reserve (DBR) in South China (Wang et al., 2019). The broadleaf forest is distributed in the core area of the reserve. The forest has not been disturbed for more than 400 years according to previous studies (Zhou et al., 2006). The mean annual precipitation is about 1678 mm, of which nearly 80% falls in the hot-humid season (from April to September) and the remainder in the dry season (from October to March). Soils in DBR are classified as Ultisols according to the USDA soil taxonomy (Soil Survey Staff, 1999). The model simulation period covered the three-year observational period (August 2009 – December 2012). Soil temperature and SWC at 10-cm depth were measured by a digital thermometer and a MPKit (ICT International, Armidale, NSW, Australia), respectively (Tang et al., 2006). The SWC was converted to soil water potential (SWP) using a soil water retention

Table 2
Governing equation for soil C and N pools in the MEND model.

Governing Equation	Eq#
Soil Carbon (state variable, e.g., P_1, denotes the C content):	
$\frac{dP_O}{dt} = I_{PO} + (1 - g_D)\cdot g_{PO}\cdot F_{12} - F_1$	(1)
$\frac{dP_H}{dt} = I_{PH} + (1 - g_D)\cdot(1 - g_{PO})\cdot F_{12} - F_2$	(2)
$\frac{dM}{dt} = (1 - f_D)\cdot(F_1 + F_2) - F_3$	(3)
$\frac{dQ}{dt} = F_4 - F_5$	(4)
$\frac{dD}{dt} = I_D + f_D\cdot(F_1 + F_2) + F_3 + g_D\cdot F_{12} + F_{14} - F_6 - (F_4 - F_5)$	(5)
$\frac{dBA}{dt} = F_6 - (F_7 - F_8) - (F_9 + F_{10} + F_{11}) - F_{14} - F_{15}$	(6)
$\frac{dBD}{dt} = (F_7 - F_8) - (F_{12} + F_{13})$	(7)
$\frac{dEP_O}{dt} = F_{15,EP1} - F_{16,EP1}$	(8)
$\frac{dEP_H}{dt} = F_{15,EP2} - F_{16,EP2}$	(9)
$\frac{dEM}{dt} = F_{15,EM} - F_{16,EM}$	(10)
$\frac{dCO_2}{dt} = R_h = (F_9 + F_{10} + F_{11}) + (F_{12} + F_{13})$	(11)
$\frac{d}{dt}(P_O + P_H + M + Q + D + BA + BD + EP_O + EP_H + EM) = (I_{PO} + I_{PH} + I_D) - (F_9 + F_{10} + F_{11}) - (F_{12} + F_{13})$	(12)
Soil Nitrogen (state variable, e.g., PN_O, denotes the N content):	
For PN_O, PN_H, MN, QN, and DN, the N flux is calculated as: $FN_i = F_i/CN_{source}$ where F_i is the C flux, and CN_{source} is the C:N ratio of the (upstream) source pool	(13)
$\frac{dBAN}{dt} = \frac{F_6}{CN_D} - \left(\frac{F_7}{CN_{BA}} - \frac{F_8}{CN_{BD}}\right) - \frac{F_{12}}{CN_{BA}} - \frac{F_{13}}{CN_{ENZ}} - FN_{mn,BA} + (FN_{im,NH4\to BA} + FN_{im,NO3\to BA})$	(14)
$\frac{dBDN}{dt} = \left(\frac{F_7}{CN_{BA}} - \frac{F_8}{CN_{BD}}\right) - FN_{mn,BD}$	(15)
$\frac{dNH_4}{dt} = I_{NH4} + (FN_{mn,BA} + FN_{mn,BD}) - FN_{im,NH4\to BA} - FN_{nit}$	(16)
$\frac{dNO_3}{dt} = I_{NO3} + FN_{nit} - FN_{nit-denit} - FN_{denit} - FN_{im,NO3\to BA}$	(17)
$\frac{d}{dt}(PN_O + PN_H + MN + QN + DN + BAN + BDN + EPN_O + EPN_H + EMN + NH_4 + NO_3) = (IN_{PO} + IN_{PH} + IN_D + I_{NH4} + I_{NO3}) - (FN_{nit-denit} + FN_{denit})$	(18)

The state variables (C and N pools) are described in Table 1; Eq. 11 indicates the total heterotrophic respiration (R_h) flux. Eq. 12 and 18 expresses the overall mass balance of C and N, respectively. The transformation fluxes (F or FN) are elucidated by Eqs. 19–41 in Table 3.

curve characterized by the van Genuchten model (van Genuchten, 1980). Monthly N deposition rates were measured from 2009 to 2012. The average total (wet + dry) NH_4^+ and NO_3^- deposition rates were 2.1 and 1.2 g N m^{-2} yr^{-1}, respectively. Soil respiration was measured using the Li-8100 Automated Soil CO_2 Flux System (Li-Cor Inc., Lincoln, NE, USA). Microbial biomass C and N were determined by the fumigation-extraction method (Wu et al., 1990). Ammonium and nitrate were extracted with 2 M KCl and determined with a Flow Injection Analysis Automated Ion Analyzer (QuickChem 8000, LACHAT, USA). In summary, there were 49 data points of heterotrophic respiration rate (R_h), 12 data points of microbial biomass C (MBC), 7 measurements of microbial C:N ratios (MB_{CN}), and 7 extractable NH_4^+ and NO_3^- concentrations.

2.4. Model calibration

We calibrated the MEND parameters controlling SOM decomposition using observed R_h and MBC in previous study (Wang et al., 2019). In the current study, we further calibrated the MEND parameters related to N mineralization, immobilization, nitrification, and denitrification (Parameter 30–35 in Table 4) using observed data including SOM C:N ratio (SOM_{CN}), MB_{CN}, and extractable NH_4^+ and NO_3^- concentrations. The model calibration period covered from August 2009 to December 2012. We used the modified Shuffled Complex Evolution (SCE) algorithm to implement multi-objective calibration of selected parameters (Duan et al., 1992; Wang et al., 2015). We minimized the overall objective function (J) as the weighted average of multiple objectives:

$$J = \sum_{i=1}^{m} w_i \cdot J_i \tag{47a}$$

$$\sum_{i=1}^{m} w_i = 1,\ w_i \in [0,\ 1] \tag{47b}$$

where $m = 4$ in this study and denotes the number of objectives and w_i is the weighting factor for the i^{th} ($i = 1,2,\ldots,m$) objective (J_i), i.e., SOM_{CN}, MB_{CN}, NH_4^+ or NO_3^- concentrations in this study (Table 5).

Each objective evaluates the goodness-of-fit of a specific observed variable (Table 5). The goodness-of-fit may be evaluated by *MARE* and/or $|PBIAS|$:

$$MARE = \frac{1}{n}\sum_{i=1}^{n}\left|\frac{Y_{sim}(i) - Y_{obs}(i)}{Y_{obs}(i)}\right| \tag{48}$$

$$|PBIAS| = \left|\frac{\bar{Y}_{sim} - \bar{Y}_{obs}}{\bar{Y}_{obs}}\right| \tag{49}$$

where *MARE* is the Mean Absolute Relative Error (MARE) and lower *MARE* values ($MARE \geq 0$) are preferred (Wang et al., 2019). *MARE* represents the averaged deviations of predictions (Y_{sim}) from their observations (Y_{obs}). *PBIAS* is the percent bias between simulated and observed mean values (Wang et al., 2018), where n is the number of data; Y_{obs} and Y_{sim} are observed and simulated values, respectively; and $\bar{Y}_{obs}$ and $\bar{Y}_{sim}$ are the mean value for Y_{obs} and Y_{sim}, respectively.

2.5. Scenarios to examine soil C-N responses to different SMRFs and forcing data

We designed three sets of numerical experiments to examine soil C-N responses to different SMRFs and forcing data. The first set (Scenario F0–F4, see Table 6) was designed to explore if different SMRFs would result in significant differences in modeling results. We assigned different SMRFs to POM_O decomposition, POM_H and MOM decomposition,

Table 3
Component fluxes in the MEND model (parameters are described in Table 4).

Flux description	Equation	Eq#
Particulate organic matter (POM) pool (oxidative) (P_O) decomposition (F_1)	$F_1 = \frac{Vd_{PO} \cdot EP_O \cdot P_O}{K_{PO} + P_O}$	(19)
POM pool (hydrolytic) (P_H) decomposition	$F_2 = \frac{Vd_{PH} \cdot EP_H \cdot P_H}{K_{PH} + P_H}$	(20)
Mineral-associated organic matter (MOM, M) decomposition	$F_3 = \frac{Vd_M \cdot EM \cdot M}{K_M + M}$	(21)
Adsorption (F_4) and desorption (F_5) between dissolved organic matter (DOM, D) and adsorbed DON (QOM, Q)	$F_4 = k_{ads} \cdot (1 - Q/Q_{max}) \cdot D$; $F_5 = k_{des} \cdot (Q/Q_{max})$	(22) (23)
DOM (D) uptake by microbes	$F_6 = \frac{1}{Y_g}(V_g + V_m) \cdot \frac{BA \cdot D}{K_D + D}$	(24)
Dormancy (F_7) and reactivation (F_8) between active (MB_A, BA) and dormant (MB_D, BD) microbes	$F_7 = [1 - D/(K_D + D)] \cdot V_m \cdot BA$; $F_8 = [D/(K_D + D)] \cdot V_m \cdot BD$	(25)(26)
MB_A (BA) growth respiration (F_9) and maintenance respiration (F_{10})	$F_9 = \left(\frac{1}{Y_g} - 1\right) \cdot \frac{V_g \cdot BA \cdot D}{K_D + D}$; $F_{10} = \left(\frac{1}{Y_g} - 1\right) \cdot \frac{V_m \cdot BA \cdot D}{K_D + D}$	(27) (28)
MB_A (BA) overflow respiration (F_{11})	$F_{11} = max\{0, BA - BAN \cdot CN_{BA,max}\}$	(29)
MB_D (BD) maintenance respiration (F_{12})	$F_{12} = \beta \cdot V_m \cdot BD$	(30)
MB_D (BD) overflow respiration (F_{13})	$F_{13} = max\{0, BD - BDN \cdot CN_{BA,max}\}$	(31)
MB_A (BA) mortality	$F_{14} = \gamma \cdot V_m \cdot BA$	(32)
Synthesis of enzymes for P_O (EP_O, $F_{15,EPO}$), enzymes for P_H (EP_H, $F_{15,EPH}$), and enzymes for M (EM, $F_{15,EM}$)	$F_{15,EPO} = P_O/(P_O + P_H) \cdot p_{EP} \cdot V_m \cdot BA$; $F_{15,EPH} = P_H/(P_O + P_H) \cdot p_{EP} \cdot V_m \cdot BA$; $F_{15,EM} = fp_{EM} \cdot p_{EP} \cdot V_m \cdot BA$; $F_{15} = F_{15,EPO} + F_{15,EPH} + F_{15,EM}$	(33)
Turnover of enzymes (EP_O, EP_H, EM)	$F_{16,EPO} = r_E \cdot EP_O$; $F_{16,EPH} = r_E \cdot EP_H$ $F_{16,EM} = r_E \cdot EM$; $F_{16} = F_{16,EPO} + F_{16,EPH} + F_{16,EM}$	(34)
N immobilization by microbes	$FN_{im,NH4 \to BA} = \frac{(VN_{im,NH4} \cdot YN_g) \cdot BA \cdot NH_4}{KS_{NH4} \cdot \left(1 + \frac{NH_4}{KS_{NH4}} + \frac{NO_3}{KS_{NO3}} + \frac{BA}{KS_{NH4}}\right)}$; $FN_{im,NO3 \to BA} = \frac{(VN_{im,NO3} \cdot YN_g) \cdot BA \cdot NO_3}{KS_{NO3} \cdot \left(1 + \frac{NH_4}{KS_{NH4}} + \frac{NO_3}{KS_{NO3}} + \frac{BA}{KS_{NO3}}\right)}$	(35) (36)
N mineralization	$FN_{mn,BA} = (1 - YN_g) \cdot FN_6$; $YN_g = \left(\frac{CN_{BA} - CN_{BA,min}}{CN_{BA,max} - CN_{BA,min}}\right)^{\omega}$	(37) (38)
Nitrification	$FN_{nit} = VN_{nit} \cdot NH_4$	(39)
Nitrifier Denitrification	$FN_{nit-denit} = FN_{nitrif} \cdot [1 - f(O_2)]$; $f(O_2) = \frac{(1 - WFP)^{4/3}}{0.5^{4/3} + (1 - WFP)^{4/3}}$ *WFP* is water-filled porosity	(40a) (40b)
Denitrification	$FN_{denit} = VN_{denit} \cdot NO_3$	(41)

microbial mortality, dormancy and resuscitation (Table 6). We conducted long-term MEND simulations beyond the calibration period (2009–2012) by repeatedly using the dynamic forcing data from the calibration period. We calculated the mean concentrations of SOC, mineral N (i.e., MN = NH_4^+ + NO_3^-), active microbial biomass C (Active-MBC) after the model reached the dynamic steady state. We then calculated the active fraction of microbial biomass (%Active-MBC) under each scenario, percent change in SOC (%ΔSOC) and mineral N (%ΔMN) relative to the SOC and MN under baseline scenario (F0).

The second set (Scenario D0–D4, see Table 7) was to investigate if model simulations with constant (time-invariant) data (litter input, soil temperature and moisture) would be different from those with dynamic (time-variant) data. The constant and dynamic data for modeling are shown in Fig. 3. We first run the model with Scenario D0 (i.e., constant litter input, soil temperature and moisture, see Table 7) to reach the steady state, following which, we then run MEND under Scenario D1–D4 (Table 7) to reach a new dynamic steady state. We then calculated Active-MBC and %Active-MBC under each scenario, and %ΔSOC and %ΔMN relative to the SOC_{SS} and MN_{SS} under baseline scenario (D0). Here we asked whether there would be significant changes between simulations driven by constant and dynamic data, whereas we did not intend to provide accurate estimates for the steady-state C and N contents such as SOC_{SS} and MN_{SS}. The reason is that the first steady state in all scenarios was determined by model calibration and simulations with constant data (i.e., litter input, soil temperature and moisture), followed by which a new steady state was achieved by varying one of the data categories (Scenario D1–D3) or varying all data (D4).

The third set of experiments (Table 8) was to examine whether the effects of litter addition on soil C and N would be different when constant (Scenario L0) or dynamic (Scenario L1) data (litter input, N deposition, soil temperature and moisture) were used. For each of the two scenarios, we designed two treatments: a control treatment with observed litter input rate (mean rate for Scenario L0 and time-variant rate for Scenario L1) and a litter-addition treatment with +11% more litter input than the control treatment. Regarding Scenario L0, we first run the model with constant data to reach the steady state. We then run MEND with litter addition, i.e., by +11% as described in Wang et al. (2019), to reach a new steady state. As per Scenario L1 with dynamic data, we also run MEND with litter addition (+11%) to reach a new dynamic steady state following the first steady state achieved by dynamic data. For each scenario with constant or dynamic data, %ΔSOC and %ΔMN were calculated as the percent changes in SOC_{SS} and MN_{SS} between the two steady states, i.e., the two treatments (litter-addition vs. control).

Table 4
MEND model parameters.

ID	Parameter	Description	Range	Units	Eq#
1	LF_0	Initial fraction of P_O, $LF_0 = P_O/(P_O + P_H)$	(0.1, 1.0)	—	
2	r_0	Initial active fraction of microbes, $r_0 = BA/(BA + BD)$	(0.01, 1)	—	
3	$fINP$	Scaling factor for litter input rate	(0.1, 0.9)	—	
4	Vd_{PO}	Maximum specific decomposition rate for P_O	(0.1, 100)	mg C mg^{-1}C h^{-1}	19
5	Vd_{PH}	Maximum specific decomposition rate for P_H	(0.1, 100)	mg C mg^{-1}C h^{-1}	20
6	Vd_M	Maximum specific decomposition rate for M	(0.1, 100)	mg C mg^{-1}C h^{-1}	21
7	K_{PO}	Half-saturation constant for P_O decomposition	(40,100)	mg C cm^{-3} soil	19
8	K_{PH}	Half-saturation constant for P_H decomposition	(1,40)	mg C cm^{-3} soil	20
9	K_M	Half-saturation constant for M decomposition	(100, 1000)	mg C cm^{-3} soil	21
10	Q_{max}	Maximum sorption capacity	(0.5, 5.0)	mg C cm^{-3} soil	22
11	K_{ba}	Binding affinity, Sorption rate $k_{ads} = k_{des} \times K_{ba}$	(1, 16)	(mg C cm^{-3} soil) $^{-1}$	22
12	k_{des}	Desorption rate	(1e-4, 0.01)	mg C cm^{-3} soil h^{-1}	23
13	r_E	Turnover rate of EP_O, EP_H, and EM	(1e-4, 0.01)	mg C mg^{-1}C h^{-1}	34
14	p_{EP}	$[V_m \times p_{EP}]$ is the production rate of EP ($EP_O + EP_H$), V_m is the specific maintenance rate for BA	(1e-4, 0.05)	—	33
15	fp_{EM}	$fp_{EM} = p_{EM}/p_{EP}$, $[V_{mt} \times p_{EM}]$ is the production rate of EM	(0.5, 3.0)	—	33
16	f_D	Fraction of decomposed P_O and P_H allocated to D	(0.05, 1)	—	3
17	g_D	Fraction of dead BA allocated to D	(0.01, 1)	—	1
18	g_{PO}	$(1 - g_D) \cdot g_{PO}$is the fraction of dead BA entering P_O	(0.05, 0.2)		1
19	V_g	Maximum specific uptake rate of D for growth	(1e-3, 0.1)	mg C mg^{-1}C h^{-1}	24
20	α	$= V_m/(V_g + V_m)$	(0.01, 0.5)	—	24
21	K_D	Half-saturation constant for microbial uptake of D	(1e-4, 0.5)	mg C cm^{-3} soil	24
22	$Y_g(T_{ref})$	True growth yield at reference temperature (T_{ref})	(0.1, 0.6)	—	24
23	k_{Yg}	Slope for Y_g dependence of temperature	(0.001, 0.016)	1/°C	24
24	Q_{10}	Q_{10} for temperature response function	(1.2, 2.5)	—	
25	γ	Max microbial mortality rate $= V_m \times \gamma$	(0.1, 20)	—	32
26	β	Ratio of dormant maintenance rate to V_m	(5e-4, 0.05)	—	30
27	ψ_{A2D}	Soil water potential (SWP) threshold for microbial dormancy; both ψ_{A2D} & $\psi_{D2A} < 0$	(–0.6, –0.2)	MPa	49
28	τ	$\psi_{D2A} = \psi_{A2D} \times \tau$, ψ_{D2A} is the SWP threshold for microbial resuscitation	(0.1, 0.9)	—	50
29	ω	Exponential in SWP function for microbial dormancy or resuscitation	(1,6)	—	50
30	$VN_{im,NH4}$	Max specific immobilization rate for NH_4^+	(0.001,0.05)	mg N mg^{-1}C h^{-1}	35
31	$VN_{im,NO3}$	Max specific immobilization rate for NO_3^-	(0.001,0.05)	mg N mg^{-1}C h^{-1}	36
32	KS_{NH4}	Half-saturation constant for NH_4^+ immobilization	(1e-4, 0.1)	mg N cm^{-3} soil	35
33	KS_{NO3}	Half-saturation constant for NO_3^- immobilization	(1e-4, 0.1)	mg N cm^{-3} soil	36
34	VN_{nit}	Max nitrification rate	(0.001, 0.1)	h^{-1}	39
35	VN_{denit}	Max denitrification rate	(0.001, 0.5)	h^{-1}	41

Notes: The column "Eq#" lists the major equation # where each parameter is used.

3. Results and discussion

3.1. Model calibration with N data

We have shown good performances in simulating R_h and MBC by the C-only MEND model in previous study (Wang et al., 2019). Our calibration of the C-N coupled MEND model also achieved good agreement between simulated and observed SOM_{CN}, MB_{CN}, NH_4^+ and NO_3^- concentrations (Fig. 4). The simulated mean SOM_{CN} was 13.8, which was only 6% higher than the observed value (Fig. 4a). The simulated daily data during 2009–2012 showed MB_{CN} between 5.9 and 7.6 and the mean MB_{CN} was consistent with the observed MB_{CN} (Fig. 4a). The simulated MB_{CN} (7 data points) exhibited a much smaller variation than the observations, mostly because there was one measurement of $MB_{CN} = 13.8$ in August 2011, which was much higher than the other 6 observed MB_{CN} values (4.5–7.7). In addition, the simulated soil NH_4^+ and NO_3^- concentrations also agreed well with the observations, with NO_3^- exhibiting a larger variation in model simulations than in observations (Fig. 4b). We did not explicitly simulate NO_3^- leaching and plant uptake of NH_4^+ and NO_3^- as no data were available for

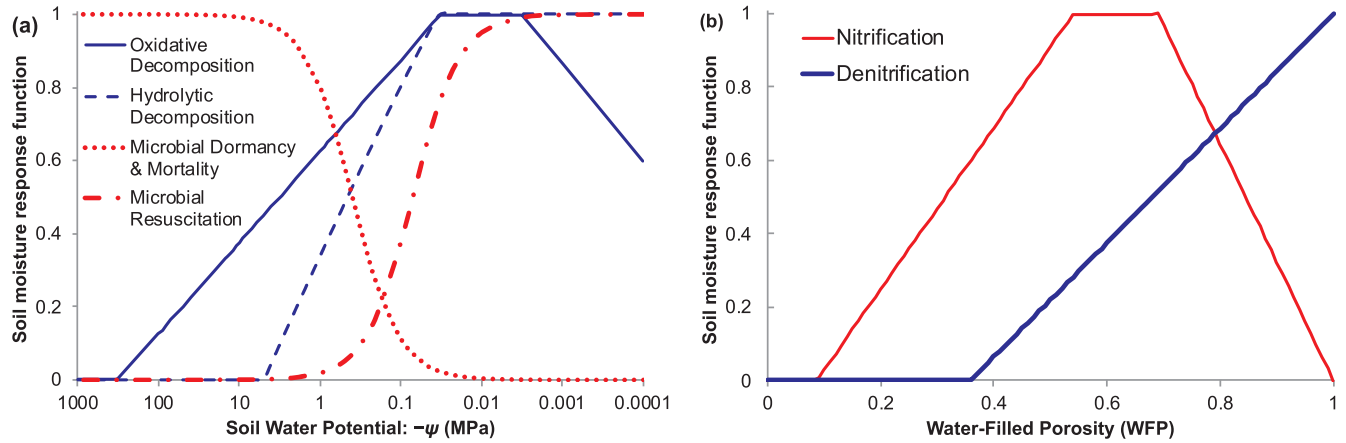

Fig. 2. Soil moisture response functions for (a) oxidative and hydrolytic decomposition, microbial dormancy & mortality and resuscitation; (b) nitrification and denitrification.

Table 5
Objective functions for MEND model parameterization.

Response Variable	Description	Objective Function
SOM_{CN}	Soil organic matter C:N ratio	$J_1 = \|PBIAS\|$
MB_{CN}	Microbial biomass C:N ratio	$J_2 = 0.5 \times \|PBIAS\| + 0.5 \times MARE$
NH_4^+	Ammonium concentration	$J_3 = 0.5 \times \|PBIAS\| + 0.5 \times MARE$
NO_3^-	Nitrate concentration	$J_4 = 0.5 \times \|PBIAS\| + 0.5 \times MARE$

Notes: *MARE* is the mean absolute relative error (Eq. (48)). $|PBIAS|$ denotes the absolute value of percent bias (Eq. (49)).

validation. However, our nitrification and denitrification simulations implicitly included these fluxes since we constrained the model by using observed SOM_{CN}, MB_{CN}, NH_4^+ or NO_3^- concentrations in addition to R_h and MBC.

3.2. Soil microbes and C-N in response to different soil moisture response functions (SMRFs)

In Fig. 5a, we showed the percent changes in SOC (%ΔSOC) and mineral N (%ΔMN) under Scenario F1–F4 with different SMRFs relative to the SOC and MN under baseline scenario F0 with default SMRFs. Without consideration of the soil moisture effects on microbial dormancy and resuscitation (Scenario F1 in Table 6), the steady-state SOC (SOC_{SS}) would increase significantly by 226% compared to the baseline (Scenario F0) SOC_{SS} (Fig. 5a). No SMRFs to modify microbial dormancy and resuscitation rates also resulted in negative change in mineral N concentration (%ΔMN = –7%). This could be explained by the lowest Active-MBC and %Active-MBC under Scenario F1 among all scenarios, consequently resulting in the lowest microbial and enzyme activities and the accumulation of SOC under Scenario F1. The low Active-MBC and SOM decomposition rate under Scenario F1 further led to less net N mineralization fluxes (by –35%) and reduced mineral N. When soil moisture effect was not considered for microbial dormancy and reactivation under Scenario F1, substrate (i.e., DOC) limitation became dominant and caused higher dormancy rates than resuscitation rates in early stage of the simulation period, ultimately resulting in low Active-MBC and %Active-MBC. In other word, when soil moisture effect was combined with the effect of substrate availability, it could lead to higher resuscitation rates than dormancy rates under wet conditions, which alleviated the single substrate-limiting effect to some extent (Scenario F0).

There were no changes in SOC, MN, and Active-MBC when the same SMRF (Eq. (43)) was applied to both oxidative and hydrolytic decomposition processes (Scenario F2) (Fig. 5a). This was expected due to all observed SWP values in the study site being lower than –0.003 MPa (or SWC < 0.494, Fig. 3c), which was not able to cause significant effects on soil microbial and C-N dynamics between the two SMRFs shown in Fig. 2a. We anticipated there might be changes in soil C-N under Scenario F2 if the soil moisture data could cover the range beyond (greater than) –0.003 MPa in Fig. 2a, because saturation of soil moisture would depress the activity of oxidative enzymes due to oxygen limitation (Freeman et al., 2001). A single SMRF like Eq. (43) has often been used to modify the decomposition rates of all soil C pools (Liang, 2019; Oleson, 2013), partly due to the generally low occurrence probability for extremely high or low soil moisture, as well as the difficulty in differentiating the soil moisture effects between multiple decomposition processes.

We also found significant increases in SOC_{SS} when the function (1–fSM2) (fSM2 denotes Eq. (43)) was assigned to microbial mortality and dormancy and the function fSM2 assigned to microbial resuscitation (Scenario F3 and F4) (Fig. 5a). However, these positive effects were much smaller than the effect by Scenario F1, owing to the Active-MBC concentrations and microbial activities under Scenario F3 and F4 were lower than those under F0 but higher than those under F1.

The above analyses in terms of different SMRFs indicated that the selection of SMRFs could lead to significant differences in model simulations of soil microbial and C-N processes. Particularly, remarkable differences in soil C and N cycling could occur between with and without accounting for the soil moisture effects on microbial dormancy and resuscitation (Scenario F1 vs. F0 in Fig. 5a), as microbial physiological states will switch under favorable or stressful environmental conditions (Bär et al., 2002; Stolpovsky et al., 2011; Wang et al., 2019).

3.3. Constant versus dynamic litter input, soil temperature or moisture

Among the four scenarios (D1–D4) with constant and/or dynamic data (litter input, soil temperature and moisture), only the scenarios with dynamic soil moisture caused significant changes in SOC_{SS} and MN_{SS} compared to those under the baseline scenario D0 with constant litter input, soil temperature and moisture (Fig. 5b). The %ΔSOC was 73% and 88%, under Scenario D3 (dynamic soil moisture) and D4 (dynamic litter input, soil temperature and moisture), respectively. Our results showed that under Scenarios D0–D2 without soil moisture dynamics, Active-MBC and %Active-MBC were almost the same, with nearly all microbes being active (%Active-MBC = %98) due to no water stress when the constant SWC (0.253) was used for modeling. However, dynamic soil moisture resulted in lower Active-MBC and more reasonable %Active-MBC (31%) and consequently reduced microbial and enzyme activities, further leading to the accumulation of SOC. Though the net N mineralization flux decreased by 12% (relative to Scenario D0), there was still an accumulation of mineral N (+36%) under Scenario D3 and D4 due to reduced N loss via denitrification.

The above analyses implied that the utilization of field-observed dynamic (time-variant) data, particularly dynamic soil moisture, could result in dynamic microbial community and physiology, subsequently leading to substantially different soil C and N processes. This was further evidenced by direct comparisons between experimental observations and model simulations driven by constant or dynamic data (Fig. 6). The simulated R_h agreed well with the observations (R^2 = 0.68) during 2009–2012 when the model was driven by "Dynamic LTW" (dynamic litter input, soil temperature and moisture) (Fig. 6a). When constant litter input was used, the simulated R_h values were similar to those by "Dynamic LTW", with a little bit lower R^2 = 0.63. When constant soil temperature was used, higher discrepancies exhibited between simulated and observed R_h (R^2 = 0.54), in which high R_h fluxes were generally underestimated. In addition, most of the R_h fluxes were greatly overestimated by the model driven by constant soil moistures (Fig. 6a). Consistent MBC results were modeled no matter what (constant or dynamic) litter input or soil temperature data were employed (Fig. 6b). However, the utilization of constant soil moisture resulted in significant overestimates of MBC (Fig. 6b), which elucidated the overestimated R_h fluxes (Fig. 6a). Our results indicated that seasonal variations in soil moisture play an important role in regulating microbial and C-N cycling. It is possible that significant differences would also appear when dynamic litter input or temperature data from other study sites were used, which conveys the same message that dynamic versus constant data may result in completely different modeling results even when the same model structure is used.

Table 6
Scenarios to test different soil moisture response functions (SMRFs).

Scenario	Oxidative POM decomposition	Hydrolytic POM and MOM decomposition	Microbial mortality	Microbial dormancy & resuscitation	Description
F0	fSM1	fSM2	fSM3	fSM3, fSM4	Baseline
F1	fSM1	fSM2	fSM3	NONE	No SMRFs for microbial dormancy & resuscitation
F2	fSM2	fSM2	fSM3	fSM3, fSM4	The same SMRF for oxidative and hydrolytic enzymes
F3	fSM2	fSM2	1– fSM2	fSM3, fSM4	SMRF for microbial mortality is complementary to that for decomposition
F4	fSM2	fSM2	1– fSM2	1– fSM2, fSM2	SMRF = fSM2 or (1– fSM2)

Note: fSM1 = Eq. (42), fSM2 = Eq. (43), fSM3 = Eq. (44), fSM4 = Eq. (45). The function of (1– fSM2) is complementary to fSM2.

Table 7
Scenarios to test model simulations with constant or dynamic data.

Scenario	Litter input	Soil temperature	Soil moisture
D0	Constant	Constant	Constant
D1	***Dynamic***	Constant	Constant
D2	Constant	***Dynamic***	Constant
D3	Constant	Constant	***Dynamic***
D4	***Dynamic***	***Dynamic***	***Dynamic***

Note: see Fig. 3 for constant or dynamic data.

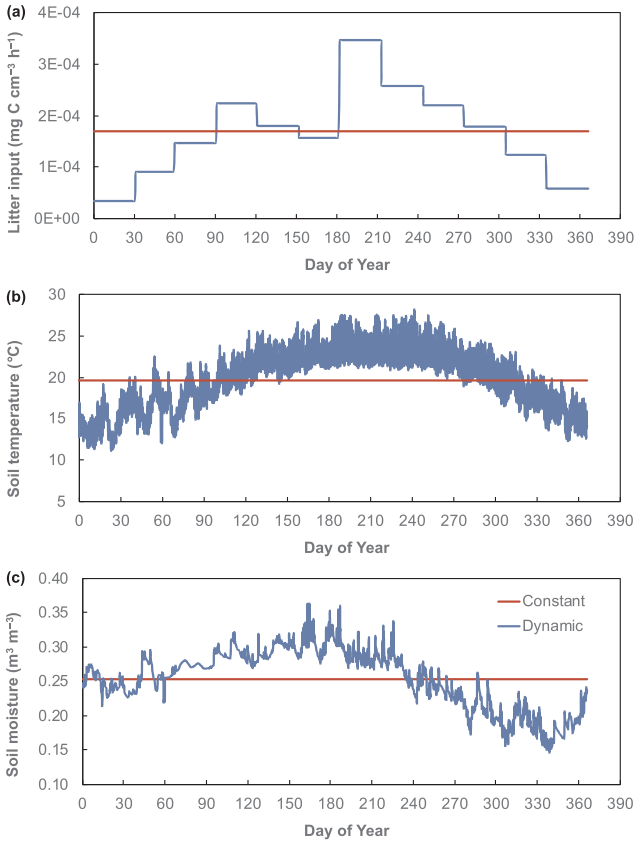

Fig. 3. Constant (time-invariant) and dynamic (time-variant) data for modeling. (a) litter input, (b) soil temperature, and (c) soil moisture.

3.4. Dynamics versus constant data result in different responses to litter addition

When constant data (litter input, N deposition, soil temperature and moisture) were used to drive model simulations, litter addition (+11%) caused positive effects on both SOC (+11%) and mineral N (+7%). However, with dynamic data as the driving force, litter addition (average of +11%) resulted in insignificant change in SOC (−2%, p-value greater than 0.05) but significant negative response in mineral N (−9%) (Fig. 7). We didn't see a significant increase in microbial biomass or active biomass, likely because almost all microbes (98%) had already become active due to no environmental stress when constant forcing data were used. As a result, the microbial and enzyme activity didn't change under litter addition, finally leading to the accumulation of SOC and mineral N. On the contrary, there was an 58% increase in Active-MBC under dynamic data and litter addition, which led to higher microbial and enzyme activities and ultimately unchanged SOC. Though both net N mineralization and denitrification slightly increased by 0.8% and 0.5%, respectively, net mineral N loss was found when dynamic data were used, due to the denitrification flux being higher than the sum of N deposition and net N mineralization. In brief, the

Table 8
Scenarios to test litter addition effects via model simulations with constant or dynamic data.

Scenario	Treatment	Litter input	Soil temperature	Soil moisture
L0	Control	Constant (observed mean)	Constant	Constant
	Litter-addition	Constant (observed + 11%)	Constant	Constant
L1	Control	***Dynamic*** (observed)	***Dynamic***	***Dynamic***
	Litter-addition	***Dynamic*** (observed + 11%)	***Dynamic***	***Dynamic***

Note: see Fig. 3 for constant or dynamic data.

responses of soil C and N to litter addition could be qualitatively different when constant or dynamic data were used to drive model simulations.

Our results highlighted the necessity to account for the seasonality of environmental factors for a better understanding of priming effects in field conditions. Priming effects often refer to the changes in the SOM decomposition caused by the addition of organic or mineral substrates, such as fresh litter, root exudates, and fertilizer (Blagodatskaya and Kuzyakov, 2008). In addition, interventions such as drying and wetting could also contribute to priming effects (Kuzyakov et al., 2000). Both positive and negative SOC responses to litter addition have been observed in short- and long-term experiments (Lajtha et al., 2014a; Lajtha et al., 2014b; Pisani et al., 2016; Sulman et al., 2018). When time-invariant data were employed to drive model simulations, we found a negative priming effect leading to the accumulation of SOC. On the contrary, we showed a positive priming effect (i.e., more native SOC loss via CO_2) with litter addition in this old broadleaf forest when dynamic data were used. In our previous study on a different forest (young pine forest) in the same area, we demonstrated a negative priming effect by the modeling with seasonal data. These experimental and modeling results imply that differential priming effects could appear in different ecosystems under similar or distinct environmental conditions, due to the complicated mechanisms for the changes in soil microbial community and activity in response to substrate additions and/or environmental change.

4. Conclusions

The C-N coupled MEND modeling regarding different SMRFs indicated that the selection of SMRFs for specific biogeochemical processes could result in distinct differences in model simulations of soil microbial and C-N processes. In particular, it is essential to accounting for the soil moisture effects on microbial dormancy and resuscitation, as the changes in microbial physiology under favorable or stressful conditions will exert strong controls on soil C and N dynamics. Without consideration of the soil moisture effects on microbial dormancy and resuscitation, the steady-state SOC (SOC_{SS}) would increase significantly compared to the baseline SOC_{SS}, whereas mineral N concentration would decrease. Among the four scenarios with constant and/or

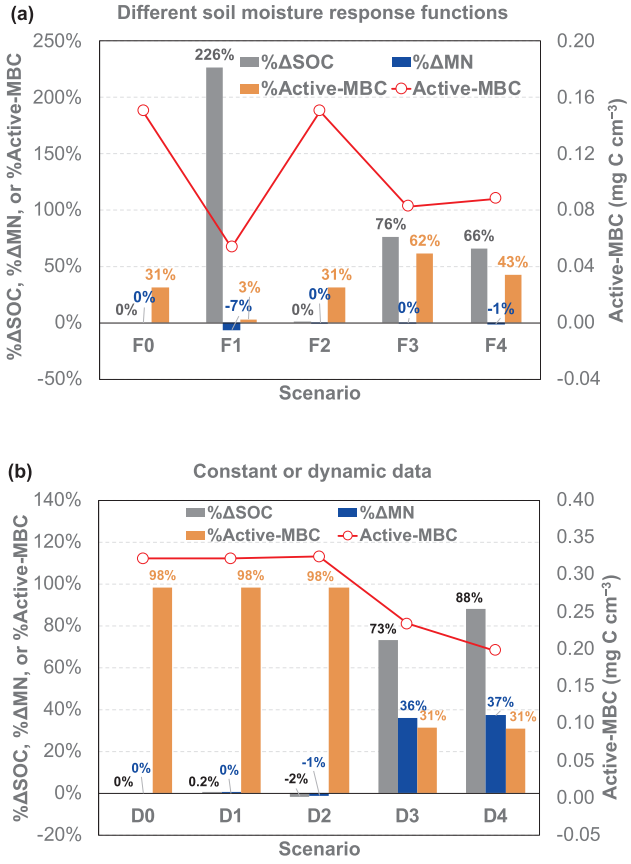

Fig. 5. (a) Percent change in soil organic C (%ΔSOC), percent change in mineral N (%ΔMN), concentration of active microbial biomass (Active-MBC), and active fraction in total biomass (%Active-MBC) when different soil moisture response functions (see scenarios in Table 6) were used. (b) %ΔSOC, %ΔMN, Active-MBC and %Active-MBC when constant or dynamic data were used (see scenarios in Table 7).

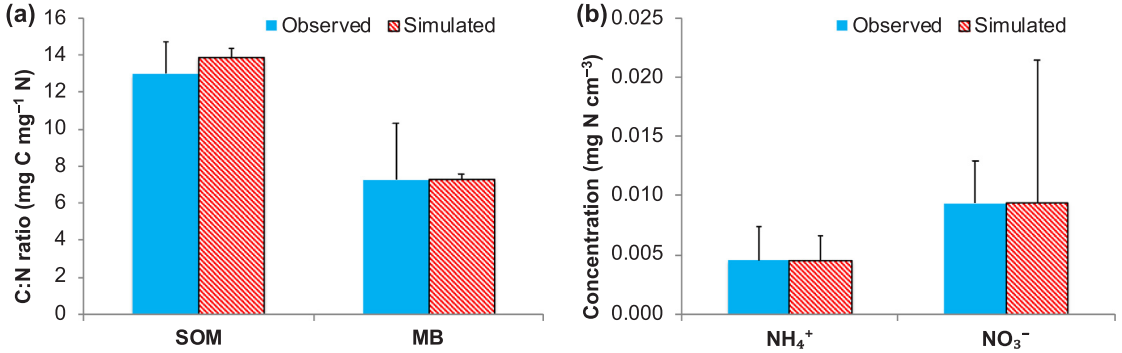

Fig. 4. Comparison between simulated and observed data. (a) C:N ratios of soil organic matter (SOM) and microbial biomass (MB); (b) Concentrations of soil NH_4^+ and NO_3^-. Error bars are standard deviations.

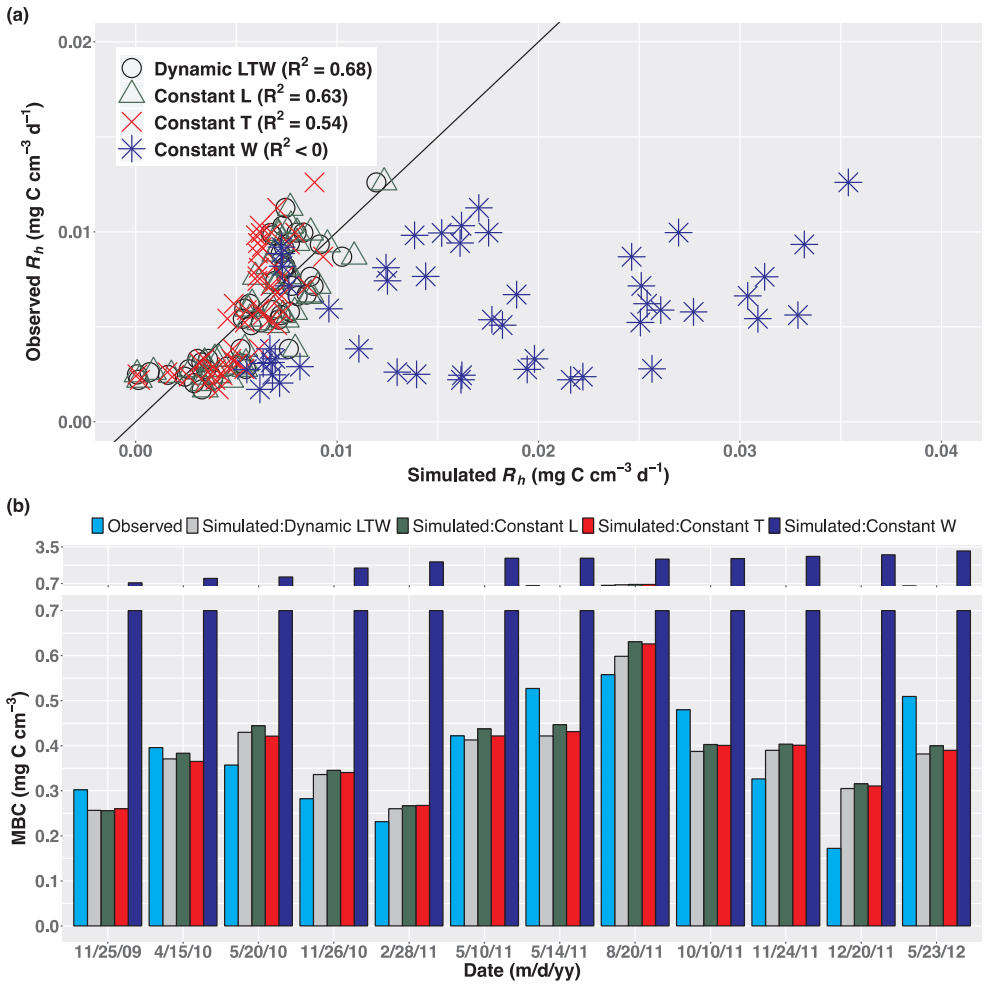

Fig. 6. Comparison between observed values and simulated values driven by "Dynamic LTW" (time-variant litter input (L), soil temperature (T) and moisture (W)), "Constant L" (time-invariant L but dynamic T and W), "Constant T" (time-invariant T but dynamic L and W), and "Constant W" (time-invariant W but dynamic L and T). (a) heterotrophic respiration (R_h) and (b) microbial biomass carbon (MBC).

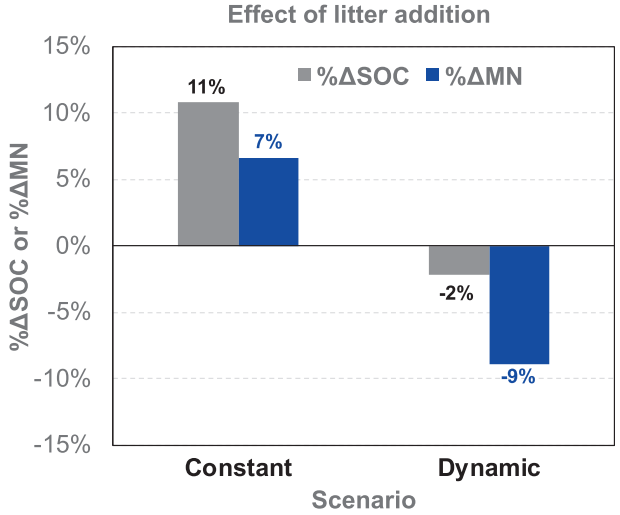

Fig. 7. Percent change in soil organic C (%ΔSOC) and mineral N (%ΔMN) as a result of litter addition when constant or dynamic data were used (see scenarios in Table 8).

dynamic data, only the scenarios with dynamic soil moisture caused significant changes in SOC_{SS} and MN_{SS} compared to those under the baseline scenario with constant data. We also show that the responses of soil C and N to litter addition could be qualitatively different when constant or dynamic data were used to drive model simulations. Therefore, we advocate the utilization of dynamic data, instead of time-invariant data, to drive model simulations and analyses. Dynamic forcing data from measurements or reanalysis better represent the real-world climate and environmental conditions, which could facilitate more realistic modeling and understanding of soil C and nutrient cycling in a changing world.

Declaration of Competing Interest

The authors declare that they have no known competing financial interests or personal relationships that could have appeared to influence the work reported in this paper.

Acknowledgements

This study was supported by the U.S. Department of Energy, Office of Science, Genomic Science Program under Award Number DE-SC0004730, DE-SC001057, DE-SC0004601, DE-SC0014079, DE-SC0016247, and DE-SC0010715, and the Office of the Vice President for Research at the University of Oklahoma. This work was also supported by the U.S. Department of Energy (DOE) Office of Biological and Environmental Research through the Terrestrial Ecosystem Science Scientific Focus Area at Oak Ridge National Laboratory (ORNL). W.H. and G.Z. were supported by the National Natural Science Foundation of

China (Grant Numbers 31670487, 41430529, and 31600353). We thank Drs. Tianfeng Han, Xiaodong Liu, Deqiang Zhang and Qianmei Zhang for conducting field experiments and data collection. ORNL is managed by the University of Tennessee-Battelle, LLC, under contract DE-AC05-00OR22725 with the U.S. DOE. Model code and data are accessible upon request at https://wanggangsheng@bitbucket.org/wanggangsheng/menddhs.git.

References

Allison, S.D., Wallenstein, M.D., Bradford, M.A., 2010. Soil-carbon response to warming dependent on microbial physiology. Nat. Geosci. 3 (5), 336–340. https://doi.org/10.1038/ngeo846.

Baldrian, P., Stursova, M., 2011. Enzymes in forest soils. In: Shukla, G., Varma, A. (Eds.), Soil Enzymology. Springer-Verlag, Berlin, Germany, Soil Biology, pp. 61–73.

Bär, M., Hardenberg, J., Meron, E., Provenzale, A., 2002. Modelling the survival of bacteria in drylands: the advantage of being dormant. Proc. R. Soc. Lond. B Biol. Sci. 269 (1494), 937–942.

Blagodatskaya, E., Kuzyakov, Y., 2008. Mechanisms of real and apparent priming effects and their dependence on soil microbial biomass and community structure: critical review. Biol. Fertil. Soils 45 (2), 115–131.

Bonan, G.B., Hartman, M.D., Parton, W.J., Wieder, W.R., 2013. Evaluating litter decomposition in earth system models with long-term litterbag experiments: an example using the Community Land Model version 4 (CLM4). Glob. Change Biol. 19 (3), 957–974. https://doi.org/10.1111/gcb.12031.

Bradford, M.A., et al., 2016. Managing uncertainty in soil carbon feedbacks to climate change. Nature Clim. Change 6 (8), 751–758. https://doi.org/10.1038/nclimate3071.

Buchkowski, R.W., Schmitz, O.J., Bradford, M.A., 2015. Microbial stoichiometry overrides biomass as a regulator of soil carbon and nitrogen cycling. Ecology 96 (4), 1139–1149.

Campo, J., Merino, A., 2016. Variations in soil carbon sequestration and their determinants along a precipitation gradient in seasonally dry tropical forest ecosystems. Glob. Change Biol. 22, 1942–1956.

Carey, J.C., et al., 2016. Temperature response of soil respiration largely unaltered with experimental warming. Proc. Natl. Acad. Sci. 113 (48), 13797–13802. https://doi.org/10.1073/pnas.1605365113.

Cleveland, C.C., Liptzin, D., 2007. C : N : P stoichiometry in soil: is there a "Redfield ratio" for the microbial biomass? Biogeochemistry 85 (3), 235–252. https://doi.org/10.1007/s10533-007-9132-0.

Criquet, S., Tagger, S., Vogt, G., Le Petit, J., 2002. Endoglucanase and β-glycosidase activities in an evergreen oak litter: annual variation and regulating factors. Soil Biol. Biochem. 34 (8), 1111–1120.

Crowther, T., et al., 2016. Quantifying global soil carbon losses in response to warming. Nature 540 (7631), 104–108.

Davidson, E.A., Samanta, S., Caramori, S.S., Savage, K., 2012. The Dual Arrhenius and Michaelis-Menten kinetics model for decomposition of soil organic matter at hourly to seasonal time scales. Glob. Change Biol. 18 (1), 371–384.

Duan, Q.Y., Sorooshian, S., Gupta, V., 1992. Effective and efficient global optimization for conceptual rainfall-runoff models. Water Resour. Res. 28 (4), 1015–1031.

Fanin, N., Fromin, N., Barantal, S., Hättenschwiler, S., 2017. Stoichiometric plasticity of microbial communities is similar between litter and soil in a tropical rainforest. Sci. Rep. 7 (1), 12498. https://doi.org/10.1038/s41598-017-12609-8.

Freeman, C., Ostle, N., Kang, H., 2001. An enzymic'latch'on a global carbon store. Nature 409 (6817) 149–149.

Frey, S.D., Lee, J., Melillo, J.M., Six, J., 2013. The temperature response of soil microbial efficiency and its feedback to climate. Nat. Clim. Change 3 (4), 395–398.

Goujard, L., Ferre, E., Gil, G., Ruaudel, F., Farnet, A., 2009. A method to quantify transesterification activities of lipases in litters. J. Microbiol. Methods 78 (2), 127–130.

Hagerty, S.B., Allison, S.D., Schimel, J.P., 2014. Accelerated microbial turnover but constant growth efficiency with warming in soil. Nature Clim. Change 4, 903–906. https://doi.org/10.1038/nclimate2361.

Halling, P.J., 1994. Thermodynamic predictions for biocatalysis in nonconventional media: theory, tests, and recommendations for experimental design and analysis. Enzyme Microb. Technol. 16 (3), 178–206.

Hansen, S., Jensen, H.E., Nielsen, N.E., Svendsen, H., 1990. DAISY-Soil plant atmosphere system model. The Royal Veterinary and Agricultural University, Copenhagen, Denmark.

Ise, T., Moorcroft, P.R., 2006. The global-scale temperature and moisture dependencies of soil organic carbon decomposition: An analysis using a mechanistic decomposition model. Biogeochemistry 80 (3), 217–231.

Kuzyakov, Y., Friedel, J., Stahr, K., 2000. Review of mechanisms and quantification of priming effects. Soil Biol. Biochem. 32 (11–12), 1485–1498.

Lajtha, K., Bowden, R.D., Nadelhoffer, K., 2014a. Litter and root manipulations provide insights into soil organic matter dynamics and stability. Soil Sci. Soc. Am. J. 78 (S1), S261–S269.

Lajtha, K., et al., 2014b. Changes to particulate versus mineral-associated soil carbon after 50 years of litter manipulation in forest and prairie experimental ecosystems. Biogeochemistry 119 (1–3), 341–360.

Li, J., et al., 2019. Reduced carbon use efficiency and increased microbial turnover with soil warming. Glob. Change Biol. 25, 900–910. https://doi.org/10.1111/gcb.14517.

Liang, J., Wang, G., Ricciuto, D.M., Gu, L., Hanson, P.J., Wood, J.D., Mayes, M.A., 2019. Evaluating the E3SM Land Model version 0 (ELMv0) at a temperate forest site using flux and soil water measurements. Geosci. Model Dev. 12, 1601–1612. https://doi.org/10.5194/gmd-12-1601-2019.

Ma, L., Shaffer, M.J., 2001. A review of carbon and nitrogen processes in nine U.S. soil nitrogen dynamics models. In: Shaffer, M.J., Ma, L. (Eds.), Modeling carbon and nitrogen dynamics for soil management. CRC Press, Boca Raton, FL, pp. 55–102.

Manzoni, S., Porporato, A., D'Odorico, P., Laio, F., Rodriguez-Iturbe, I., 2004. Soil nutrient cycles as a nonlinear dynamical system. Nonlinear Processes Geophys. 11 (5–6), 589–598.

Manzoni, S., Schaeffer, S.M., Katul, G., Porporato, A., Schimel, J.P., 2014. A theoretical analysis of microbial eco-physiological and diffusion limitations to carbon cycling in drying soils. Soil Biol. Biochem. 73, 69–83. https://doi.org/10.1016/j.soilbio.2014.02.008.

Manzoni, S., Schimel, J.P., Porporato, A., 2012a. Responses of soil microbial communities to water stress: results from a meta-analysis. Ecology 93 (4), 930–938.

Manzoni, S., Taylor, P., Richter, A., Porporato, A., Agren, G.I., 2012b. Environmental and stoichiometric controls on microbial carbon-use efficiency in soils. New Phytol. 196 (1), 79–91. https://doi.org/10.1111/j.1469-8137.2012.04225.x.

Mooshammer, M., Wanek, W., Hämmerle, I., Fuchslueger, L., Hofhansl, F., Knoltsch, A., Schnecker, J., Takriti, M., Watzka, M., Wild, B., 2014. Adjustment of microbial nitrogen use efficiency to carbon: nitrogen imbalances regulates soil nitrogen cycling. Nature Communications 5, 3694. https://doi.org/10.1038/ncomms4694.

Moyano, F.E., Manzoni, S., Chenu, C., 2013. Responses of soil heterotrophic respiration to moisture availability: An exploration of processes and models. Soil Biol. Biochem. 59, 72–85. https://doi.org/10.1016/j.soilbio.2013.01.002.

Muller, C., 1999. Modeling soil-biosphere interactions. CABI Publishing, New York, NY, pp. 354.

Ohashi, M., et al., 2008. Characteristics of soil CO_2 efflux variability in an aseasonal tropical rainforest in Borneo Island. Biogeochemistry 90 (3), 275–289.

Oleson, K.W., et al., 2013. Technical Description of version 4.5 of the Community Land Model (CLM). National Center for Atmospheric Research, Boulder CO.

Pisani, O., et al., 2016. Long-term doubling of litter inputs accelerates soil organic matter degradation and reduces soil carbon stocks. Biogeochemistry 127 (1), 1–14.

Rowland, L., et al., 2014. Evidence for strong seasonality in the carbon storage and carbon use efficiency of an Amazonian forest. Glob. Change Biol. 20 (3), 979–991. https://doi.org/10.1111/gcb.12375.

Sardans, J., Penuelas, J., 2005. Drought decreases soil enzyme activity in a Mediterranean *Quercus ilex* L. forest. Soil Biol. Biochem. 37 (3), 455–461.

Schimel, J., Balser, T.C., Wallenstein, M., 2007. Microbial stress-response physiology and its implications for ecosystem function. Ecology 88 (6), 1386–1394. https://doi.org/10.1890/06-0219.

Schimel, J.P., Weintraub, M.N., 2003. The implications of exoenzyme activity on microbial carbon and nitrogen limitation in soil: a theoretical model. Soil Biol. Biochem. 35 (4), 549–563. https://doi.org/10.1016/s0038-0717(03)00015-4.

Shi, Z., et al., 2015. Experimental warming altered rates of carbon processes, allocation, and carbon storage in a tallgrass prairie. Ecosphere 6 (11), 1–16.

Sistla, S.A., Schimel, J.P., 2012. Stoichiometric flexibility as a regulator of carbon and nutrient cycling in terrestrial ecosystems under change. New Phytol. 196 (1), 68–78. https://doi.org/10.1111/j.1469-8137.2012.04234.x.

Soil Survey Staff, 1999. Soil Taxonomy, A Basic System of Soil Classification for Making and Interpreting Soil Surveys. United States Department of Agriculture, Natural Resources Conservation Service, Washington, DC, 871 pp.

Stolpovsky, K., Martinez-Lavanchy, P., Heipieper, H.J., Van Cappellen, P., Thullner, M., 2011. Incorporating dormancy in dynamic microbial community models. Ecol. Model. 222 (17), 3092–3102.

Sulman, B.N., et al., 2018. Multiple models and experiments underscore large uncertainty in soil carbon dynamics. Biogeochemistry 141 (2), 109–123.

Tang, J., Riley, W.J., 2015. Weaker soil carbon-climate feedbacks resulting from microbial and abiotic interactions. Nature Clim. Change 5, 56–60. https://doi.org/10.1038/nclimate2438.

Tang, X.L., Liu, S.G., Zhou, G.Y., Zhang, D.Q., Zhou, C.Y., 2006. Soil-atmospheric exchange of CO_2, CH_4, and N_2O in three subtropical forest ecosystems in southern China. Glob. Change Biol. 12 (3), 546–560. https://doi.org/10.1111/j.1365-2486.2006.01109.x.

Thornton, P.E., Rosenbloom, N.A., 2005. Ecosystem model spin-up: Estimating steady state conditions in a coupled terrestrial carbon and nitrogen cycle model. Ecol. Model. 189 (1), 25–48.

van Genuchten, M.T., 1980. A closed-form equation for predicting the hydraulic conductivity of unsaturated soils. Soil Sci. Soc. Am. J. 44 (5), 892–898.

Wallenstein, M.D., Weintraub, M.N., 2008. Emerging tools for measuring and modeling the in situ activity of soil extracellular enzymes. Soil Biol. Biochem. 40 (9), 2098–2106.

Wang, G., Chen, S., 2013. Evaluation of a soil greenhouse gas emission model based on Bayesian inference and MCMC: Model uncertainty. Ecol. Model. 253, 97–106. https://doi.org/10.1016/j.ecolmodel.2012.09.010.

Wang, G., et al., 2019. Soil moisture drives microbial controls on carbon decomposition in two subtropical forests. Soil Biol. Biochem. 130, 185–194. https://doi.org/10.1016/j.soilbio.2018.12.017.

Wang, G., et al., 2015. Microbial dormancy improves development and experimental validation of ecosystem model. The ISME Journal 9, 226–237. https://doi.org/10.1038/ismej.2014.120.

Wang, G., Jager, H.I., Baskaran, L.M., Brandt, C.C., 2018. Hydrologic and Water Quality Responses to Biomass Production in the Tennessee River Basin. GCB Bioenergy 10 (11), 877–893. https://doi.org/10.1111/gcbb.12537.

Wang, G., Post, W.M., Mayes, M.A., 2013. Development of microbial-enzyme-mediated decomposition model parameters through steady-state and dynamic analyses. Ecol.

Appl. 23 (1), 255–272. https://doi.org/10.1890/12-0681.1.
Wang, G., Post, W.M., Mayes, M.A., Frerichs, J.T., Jagadamma, S., 2012. Parameter estimation for models of ligninolytic and cellulolytic enzyme kinetics. Soil Biol. Biochem. 48, 28–38. https://doi.org/10.1016/j.soilbio.2012.01.011.
Wrage-Mönnig, N., et al., 2018. The role of nitrifier denitrification in the production of nitrous oxide revisited. Soil Biol. Biochem. 123, A3–A16. https://doi.org/10.1016/j.soilbio.2018.03.020.
Wu, J., Joergensen, R.G., Pommerening, B., Chaussod, R., Brookes, P.C., 1990. Measurement of soil microbial biomass c by fumigation extraction – an automated procedure. Soil Biol. Biochem. 22 (8), 1167–1169.
Wu, L., McGechan, M.B., 1998. A review of carbon and nitrogen processes in four soil nitrogen dynamics models. J. Agric. Eng. Res. 69 (4), 279–305.
Zaks, A., Klibanov, A.M., 1988. The effect of water on enzyme action in organic media. J. Biol. Chem. 263 (17), 8017–8021.
Zechmeister-Boltenstern, S., et al., 2015. The application of ecological stoichiometry to plant–microbial–soil organic matter transformations. Ecol. Monogr. 85 (2), 133–155. https://doi.org/10.1890/14-0777.1.
Zhou, G., et al., 2006. Old-growth forests can accumulate carbon in soils. Science 314 (5804) 1417–1417.
Zhu, X., Burger, M., Doane, T.A., Horwath, W.R., 2013. Ammonia oxidation pathways and nitrifier denitrification are significant sources of N2O and NO under low oxygen availability. Proc. Natl. Acad. Sci. 110 (16), 6328–6333.